J Biomol NMR (2015) 63:275–282
DOI 10.1007/s10858-015-9984-x

ARTICLE

Encoded loop-lanthanide-binding tags for long-range distance measurements in proteins by NMR and EPR spectroscopy

Dominic Barthelmes[1] · Markus Gränz[2] · Katja Barthelmes[1,5] · Karen N. Allen[3] · Barbara Imperiali[4] · Thomas Prisner[2] · Harald Schwalbe[1]

Received: 17 August 2015 / Accepted: 1 September 2015 / Published online: 4 September 2015

Abstract We recently engineered encodable lanthanide binding tags (LBTs) into proteins and demonstrated their applicability in Nuclear Magnetic Resonance (NMR) spectroscopy, X-ray crystallography and luminescence studies. Here, we engineered two-loop-LBTs into the model protein interleukin-1β (IL1β) and measured ^{1}H, ^{15}N-pseudocontact shifts (PCSs) by NMR spectroscopy. We determined the $\Delta\chi$-tensors associated with each Tm^{3+}-loaded loop-LBT and show that the experimental PCSs yield structural information at the interface between the two metal ion centers at atomic resolution. Such information is very valuable for the determination of the sites of interfaces in protein–protein-complexes. Combining the experimental PCSs of the two-loop-LBT construct IL1β-S2R2 and the respective single-loop-LBT constructs IL1β-S2, IL1β-R2 we additionally determined the distance between the metal ion centers. Further, we explore the use of two-loop LBTs loaded with Gd^{3+} as a novel tool for distance determination by Electron Paramagnetic Resonance spectroscopy and show the NMR-derived distances to be remarkably consistent with distances derived from Pulsed Electron–Electron Dipolar Resonance.

Keywords Paramagnetic NMR · EPR · PELDOR · Lanthanide binding tags

Introduction

In living cells, the majority of proteins assemble into multimers forming dynamic networks with cognate binding partners (Lynch 2013). A survey of the Protein Data Bank (PDB) (Bernstein et al. 1977) reveals that structures of multi-domain proteins and protein–protein complexes solved by NMR spectroscopy are highly underrepresented compared to monomeric proteins. Recent studies (Mackereth et al. 2011; Lapinaite et al. 2013; Duss et al. 2014; Alonso-García et al. 2015) on biomacromolecules and their

D. Barthelmes, M. Gränz and K. Barthelmes have contributed equally.

Electronic supplementary material The online version of this article (doi:10.1007/s10858-015-9984-x) contains supplementary material, which is available to authorized users.

✉ Thomas Prisner
prisner@prisner.de

✉ Harald Schwalbe
Schwalbe@nmr.uni-frankfurt.de

[1] Institute of Organic Chemistry and Chemical Biology, Center for Biomolecular Magnetic Resonance, Goethe University Frankfurt, Max-von-Laue-Straße 7, 60438 Frankfurt Am Main, Germany

[2] Institute of Physical and Theoretical Chemistry, Center for Biomolecular Magnetic Resonance, Goethe University Frankfurt, Max-von-Laue-Straße 7, 60438 Frankfurt Am Main, Germany

[3] Department of Chemistry, Boston University, 590 Commonwealth Avenue, Boston, MA 02215, USA

[4] Departments of Chemistry and Biology, Massachusetts Institute of Technology, 77 Massachusetts Avenue, Cambridge, MA 02139, USA

[5] Present Address: Department of Chemistry, Munich Center for Integrated Protein Science and Chair Biomolecular NMR, Technical University Munich, Lichtenbergstrasse 4, 85747 Garching, Germany

multimers have addressed this problem using a combination of complementary methods in a "divide and conquer" strategy where structures of single domains are determined individually and assembled using long-range angular and distance restraints.

In principle, EPR and NMR spectroscopy allow the investigation of long-range angular and distance restraints by measuring PELDOR or PCSs (Göbl et al. 2014; Hass and Ubbink 2014; Duss et al. 2015). These methods require the introduction of spin-labels (Tamm et al. 2007; Schiemann and Prisner 2007; Keizers and Ubbink 2011; Yagi et al. 2011; Loscha et al. 2012; Russo et al. 2013) attached to or within a protein. In NMR- spectroscopic studies, attachment of a single paramagnetic lanthanide center (Keizers and Ubbink 2011) with an anisotropic $\Delta\chi$-tensor (Bertini et al. 2002) has been employed to obtain PCSs, which report on the distance and radial coordinates of a nuclear spin with respect to the paramagnetic center. For Gd^{3+}–Gd^{3+} PELDOR distance measurements, simultaneous two-site attachment is required and has been established using chemical tags (Raitsimring et al. 2007; Potapov et al. 2010; Gordon-Grossman et al. 2011; Lueders et al. 2011; Song et al. 2011; Yagi et al. 2011; Garbuio et al. 2013; Matalon et al. 2013).

Recently, a genetically encodable lanthanide-binding tag (LBT) was introduced, which was initially attached to the protein termini (Wöhnert et al. 2003), then extended to a double LBT (Silvaggi et al. 2007; Martin et al. 2007) and then further rigidified by insertion into loop regions of interleukin-1-beta (IL1β) (Barthelmes et al. 2011). We demonstrated the applicability of LBTs for obtaining structural restraints by paramagnetic NMR spectroscopy. The LBT consists of an amino acid sequence (Fig. 1a, b) that specifically binds trivalent lanthanide (Ln) ions with low nM affinity and the fusion LBT-protein can be produced in any suitable expression platform. Herein, we extend our approach by inserting the LBT sequence into both the R2 and S2 loop regions of the model protein IL1β (Barthelmes et al. 2011) forming the two-loop-LBT tagged protein termed IL1β-S2R2 (Fig. 1c) and show the applicability of the two-loop LBT approach for PELDOR measurements and paramagnetic NMR-spectroscopy.

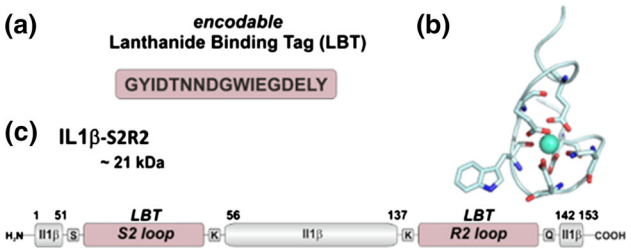

Fig. 1 **a** Amino-acid sequence of the LBT used in this study. **b** Structure representation of the folded LBT complexing a lanthanide-ion (*green sphere*) (Barthelmes et al. 2011). **c** Schematic sequence representation of the two-loop-LBT construct of IL1β with the LBT sequences *highlighted in red*. S and R correspond to the respective loop regions. In the 2-series two of the initial loop residues (DD) of IL1β were removed and the LBT sequence was inserted instead

Materials and methods

Protein expression, purification and sample preparation

^{15}N-labelled samples of the single and two-loop-LBT tagged IL1β constructs were prepared as Glutathione *S*-transferase (GST) fusion proteins in BL21(DE3) *Escherichia coli* cells grown in autoinducing medium (P-5052) (Studier 2005). After cell lysis using a Microfluidizer® system (Microfluidics, Westwood, MA 02090 USA), the GST fusion proteins were extracted from the supernatant using GST affinity chromatography, cleaved with tobacco etch virus (TEV) protease and further purified using size-exclusion chromatography. Samples were concentrated to 50 μM in 10 mM HEPES, pH 7.0, 100 mM NaCl and 5 mM β-mercaptoethanol and loaded by careful titration with 10 aliquots of 0.11 equivalents of the paramagnetic (Tb^{3+}, Tm^{3+}, Dy^{3+}) or diamagnetic lanthanide (Lu^{3+}). The final sample contained 1.1 equivalents of lanthanide and was repeatedly concentrated and diluted with fresh buffer to a final concentration of 0.2 mM using Amicon Centriprep/Centricon centrifugal concentrator devices.

NMR experiments

NMR measurements were performed in buffer containing 10 mM HEPES at pH 7.0, 100 mM NaCl, 5 mM β-mercaptoethanol, 100 μM DSS and 90/10 % H_2O/D_2O. All ^{1}H–^{15}N-HSQC spectra were recorded at 293 K on a Bruker AV600 NMR spectrometer equipped with a 5 mm TXI Cryoprobe H-C/N-D with single-axis and a Z-gradient. For diamagnetic samples, the spectral widths/acquisition times of the ^{1}H–^{15}N-HSQC spectra were set to 14 ppm/60.8 ms (^{1}H) and 28 ppm/75.2 ms (^{15}N) using 32 scans per increment. Paramagnetic spectra were recorded using a spectral width of 14 × 28 ppm in t_2 and t_1 and acquisition times of 60.8 ms (^{1}H) and 56.3 ms (^{15}N) and 96 scans per increment. For calibration of the chemical shifts in the proton dimension, 4,4-dimethyl-4-silapentane-1-sulfonic acid (DSS) was used as a reference signal. Pseudocontact shifts (PCS) were calculated as the difference of the chemical shifts in the diamagnetic and paramagnetic samples. The determination of the $\Delta\chi$-tensors and metal positions is described in the Supporting Information (SI).

EPR and PELDOR/DEER experiments

EPR measurements were performed in buffer containing 10 mM HEPES at pH 7.0, 100 mM NaCl, 5 mM β-mercaptoethanol, 100 % H_2O. Glycerol (20 %) was added to the solution for cryoprotection. Pulsed EPR data were recorded on an ELEXSYS E580 EPR spectrometer (Bruker) equipped with a PELDOR unit (E580-400U, Bruker), a continuous-flow helium cryostat (CF935, Oxford Instruments), and a temperature control system (ITC 502, Oxford Instruments). Experiments were performed at Q-band frequencies (33.7 GHz) using an ELEXSYS SuperQ-FT accessory unit and a Bruker AmpQ 10 W amplifier with a Bruker EN5107D2 cavity at 10 K. For PELDOR experiments, the dead-time free four-pulse sequence with phase-cycled π/2-pulse was used (Pannier et al. 2000). Pulse lengths were optimized to 16 ns (π/2 and π) for the observer pulses and 8 ns (π) for the pump pulse. The pump pulse was set to the maximum of the echo-detected EPR spectrum and the probe pulses were set 100 MHz higher. To obtain distance distributions, the PELDOR trace was processed to remove the background function from intermolecular interactions and the background-corrected trace was fitted with a Tikhonov regularization and Two Gaussians resulting in distance distributions, as it is implemented in the software package DeerAnalysis2013 (Jeschke et al. 2006).

Results and discussion

We recorded ^{15}N-HSQC NMR spectra of IL1β-S2R2 loaded with diamagnetic Lu^{3+} or paramagnetic Tm^{3+} at a field strength of $B_0 = 14.1$ T. The ^{1}H, ^{15}N resonance assignments of diamagnetic IL1β-S2R2 were inferred from the assignments of the respective single-loop LBT constructs IL1β-R2 and IL1β-S2 (Barthelmes et al. 2011). Metal ion binding of IL1β-S2R2 occurred in slow exchange preventing paramagnetic assignment via lanthanide titration or exchange spectroscopy. In the presence of different lanthanides, the respective cross peaks approximately resonate on diagonal lines within the ^{15}N-HSQC spectra. We therefore recorded additional ^{15}N-HSQC spectra of IL1β-S2R2 loaded with Tb^{3+} and Dy^{3+} and employed a bootstrapping assignment procedure as described previously (Barthelmes et al. 2011). Despite considerable line broadening resulting from the two paramagnetic metal ion centers, a total of 61 cross peaks in the ^{15}N-HSQC spectrum of IL1β-S2R2 loaded with Tm^{3+} could be unambiguously assigned (Figures S1 and S2), with most of the respective residues located at the interface between the metal centers (Fig. 5c). Sizeable pseudocontact shifts (PCS) ranging from −0.82 to 0.35 ppm were calculated as the difference of the diamagnetic and paramagnetic chemical shifts (Fig. 2 and Table S2).

To investigate the effect of two paramagnetic centers on the nuclear spins, we first determined the Δχ-tensors of the single-loop-LBTs constructs IL1β-S2 and –R2 individually (Fig. 3). We then calculated the PCSs for IL1β based on the hypothesis that Δχ-tensors of IL1β-R2 and -S2 are additive (Bentrop et al. 1997) in IL1β-S2R2. The correlation of the calculated PCSs to the experimental PCSs obtained for IL1β-S2R2 is remarkably good with an R^2 of 0.959 (Fig. 4) confirming the additivity of both Δχ-tensors in the two-loop-LBT construct. To obtain the lanthanide positions and the Δχ-tensors in IL1β-S2R2, we fitted the PCS against the previously refined IL1β wild-type structure (Barthelmes et al. 2011) under the assumption that the Δχ-tensors of Tm^{3+} in the R2-loop and the S2-loop are additive using a Mathematica (Wolfram Research Inc., Champaign 2014) script developed in-house (see SI). Following an approach implemented in the program *Numbat* (Schmitz et al. 2008), we assessed the error of the Δχ-tensor and metal position in a Monte-Carlo (MC) simulation, in which 30 % of the data were randomly deleted and Gaussian distributed noise was added to both the experimental PCS and the structure prior to the fit.

Following this approach, the fit of PCS solely from data derived for the IL1β-S2R2 construct loaded with Tm^{3+} did not converge stably in the MC simulation because each of the 16 fitting parameters was represented by only few PCS values. Due to the need for more data points, we combined the PCS from IL1β-S2R2, IL1β-R2 and -S2 and performed a global fit against the refined IL1β wild type structure. The MC-simulation resulted in an excellent correlation of 476 experimental and back-calculated ^{1}H, ^{15}N PCSs with an R^2 of 0.982 (Fig. 5a). Calculation of the Δχ-tensors for Tm^{3+}-loaded IL1β-S2R2 resulted in Δχ-tensor values (Fig. 5b) in the R2 loop with $\Delta\chi_{ax,\ R2} = -20.1 \times 10^{-32}$ m^3, $\Delta\chi_{rh,\ R2} = -2.2 \times 10^{-32}$ m^3 and in the S2 loop with $\Delta\chi_{ax,\ S2} = -26.3 \times 10^{-32}$ m^3, $\Delta\chi_{rh,\ s2} = -9.5 \times 10^{-32}$ m^3 which are in the range of values previously reported (Bertini et al. 2001; Schmitz et al. 2008; Barthelmes et al. 2011). Euler angles for the rotation of the Δχ-tensor from the protein frame to the *unique tensor representation* (UTR) frame (Schmitz et al. 2008) were calculated in radians for the R2 loop as $(\alpha, \beta, \gamma) = (2.7 \pm 0.3, 0.6 \pm 0.2, 1.7 \pm 0.9)$ and for the S2 loop as $(\alpha,\ \beta,\ \gamma) = (2.7 \pm 0.1,\ 0.9 \pm 0.9,\ 2.3 \pm 1.0)$. The pseudocontact shifts give the positions of the two Tm^{3+} ions with respect to the structure of IL1β. As seen in previous studies, the calculated positions of the lanthanide centers were located about 1.1 nm from the LBT insertion site. From these positions we calculated the lanthanides to be separated by a distance of 3.30 ± 0.09 nm (Fig. 5c).

We validated the Tm^{3+}–Tm^{3+} distance in IL1β-S2R2 by Gd^{3+}–Gd^{3+} PELDOR measurements and further

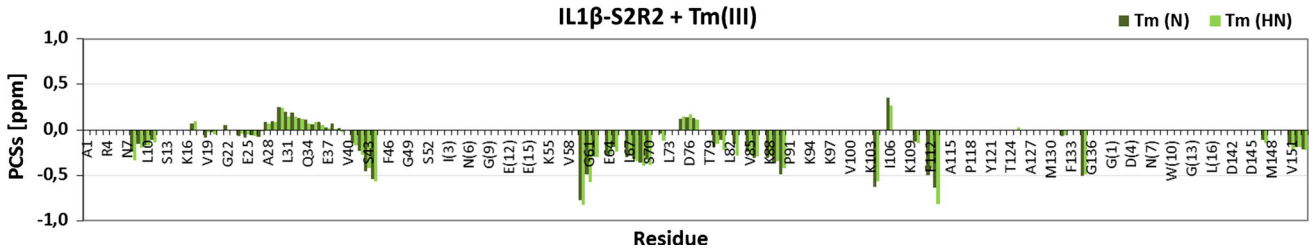

Fig. 2 Experimental ^{1}H-PCS (*light green*) and ^{15}N-PCS (*dark green*) for two-loop-LBT-IL1β-S2R2 measured using Tm^{3+} PCS were extracted from the diamagnetic (Lu^{3+}) and paramagnetic (Tm^{3+}) ^{1}H–^{15}N-HSQC NMR spectra

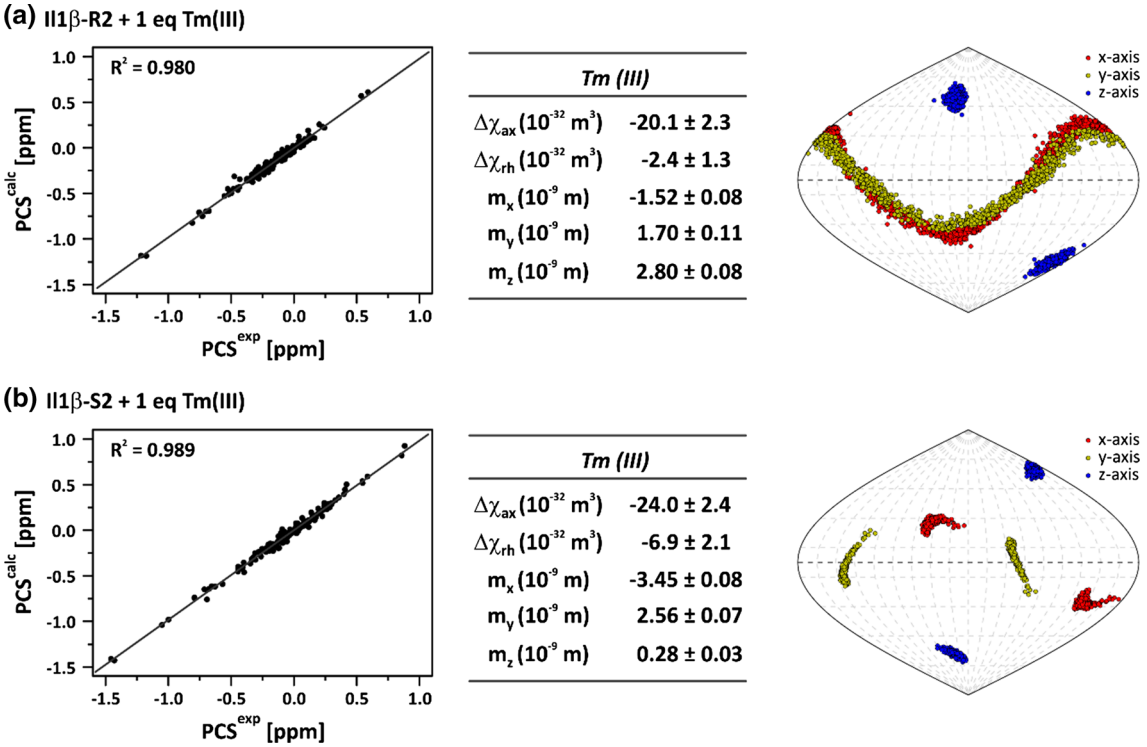

Fig. 3 Experimental PCS for single-loop-LBT- **a** IL1β-R2 and **b** IL1β-S2 each loaded with Tm^{3+} were back-calculated onto the previously RDC-refined wild type structure of IL1β

demonstrate the use of encodable LBTs for distance determination by EPR spectroscopy, which had previously been performed exclusively using chemical tags (Raitsimring et al. 2007; Potapov et al. 2010; Gordon-Grossman et al. 2011; Lueders et al. 2011; Song et al. 2011; Yagi et al. 2011; Garbuio et al. 2013; Matalon et al. 2013). We measured PELDOR at 33.4 GHz frequency (Q-band) using the two-loop-LBT mutant IL1β-S2R2. The Q-band echo detected field sweep EPR spectrum exhibited an overall width of 0.8 T (Fig. 6).

The broad EPR spectral width indicated a relatively large zero-field splitting (ZFS) of ~1.8 GHz for this Gd^{3+}-tag, which arises from the asymmetry of the LBT coordination sphere and is much larger than for Gd^{3+}-DOTA-tagged proteins (Goldfarb 2014). The width of the central transition (between the electron spin sublevels $m_s = -1/2$ to $m_s = 1/2$) defined at half height is ~39 mT. The resonator was centered at the pump frequency and a pump-probe frequency offset of 100 MHz was chosen (i) in order to suppress the influence of the pseudo-secular term of the dipolar coupling Hamiltonian, (ii) minimize partial overlap of the bandwidth of the pump- ($\pi = 8$ ns) and probe pulses ($\pi/2$ and $\pi = 16$ ns) and (iii) is the maximum width of the used resonator. Reduction of the refocused echo was observed upon application of the pump pulse, as described previously (Yulikov et al. 2012; Lueders et al. 2013). Due to the broad spectral width, a modulation depth of about 1.5 %

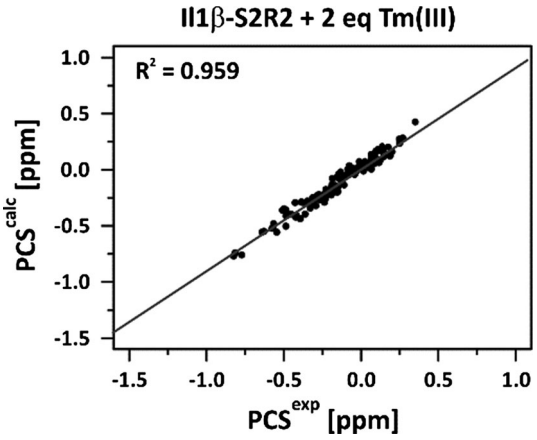

Fig. 4 Experimental PCS of IL1β-S2R2 back-calculated under the hypothesis that Δχ-tensors of IL1β-R2 and -S2 are additive in IL1β-S2R2 (tensors used for the back-calculation are shown in Fig. 2)

was achieved with a 8 ns pump pulse, optimized for the central transition. An achievement of such modulation depth is expected, as only a small fraction of the spins in the ensemble could be excited by the pump pulse. However, the relatively high echo signal intensity and a transversal relaxation time of 2.2 µs for IL1β-S2R2 (Figure S3) result in a reasonable signal-to-noise ratio. Figure 7 shows spectra applying a four-pulse PELDOR experiment of IL1β-S2R2 in buffered 80 % H_2O/20 % glycerol. The dipolar evolution time was set to 2 µs and the Q-band PELDOR time trace clearly reveals dipolar oscillations before (Fig. 7a) and after division of the background decay (Fig. 7b, black trace). Tikhonov regularization (Fig. 7b, blue trace) resulted in a distance distribution with two peaks with a maximum at 3.55 nm (Fig. 7c, blue trace). The peak at 2.50 nm is most likely an artifact that originates from the partial excitation of non-central transitions with detection pulses (Lueders et al. 2011; Yulikov et al. 2012; Goldfarb 2014). Due to the relatively large ZFS parameter D of 1.8 GHz (Fig. 6) and pump-probe frequency offset of 100 MHz, contribution from the pseudo-secular term of the dipolar coupling Hamiltonian can be neglected in the analysis of the PELDOR time trace (Dalaloyan et al. 2015). Additional fitting of the time trace with two Gaussians yields the same distance with an even smaller distribution and a broader, less intense second peak. The full width at half height (FWHH) for the maximum peak with Tikhonov regularization is only 0.5 nm and therefore remarkably good for such a system (Goldfarb 2014). Given the experimental uncertainties and different physical conditions of the sample, the Gd^{3+}–Gd^{3+} distance measurement from PELDOR is in good agreement with the distance of 3.30 ± 0.09 nm obtained by NMR spectroscopy. Note, that the inter-metal ion distance derived from NMR spectroscopy is 0.25 nm longer than the distance obtained from PELDOR measurement. While this discrepancy is not statistically significant, it is worth noting that differences in the observation of molecular dynamics by PELDOR and PCS may contribute to the measurement difference. However, the current accuracy of the NMR and PELDOR data is not sufficient to define inconsistencies with a static structure of IL1β.

In summary, we show for a rigid biomacromolecular model system engineered with two-loop-LBTs that their Δχ-tensors are additive and provide structural information at the interface between the two metal ion centers at atomic resolution. Such information is valuable for the determination of structures of multi-domain proteins and protein–protein complexes. In our case, we required additional data from proteins with a single LBT for the precise determination of the tensor parameters. Yet, the

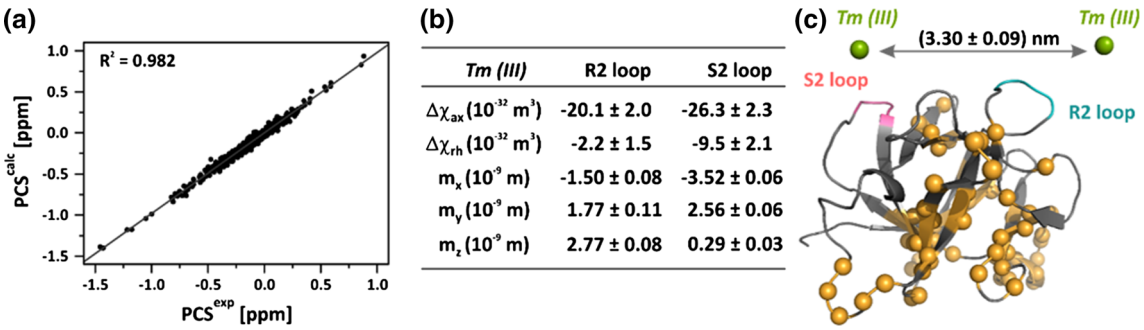

Tm (III)	R2 loop	S2 loop
$\Delta\chi_{ax}$ (10^{-32} m^3)	-20.1 ± 2.0	-26.3 ± 2.3
$\Delta\chi_{rh}$ (10^{-32} m^3)	-2.2 ± 1.5	-9.5 ± 2.1
m_x (10^{-9} m)	-1.50 ± 0.08	-3.52 ± 0.06
m_y (10^{-9} m)	1.77 ± 0.11	2.56 ± 0.06
m_z (10^{-9} m)	2.77 ± 0.08	0.29 ± 0.03

Fig. 5 Determination of Δχ-tensors and metal position in the two-loop-LBT IL1β-S2R2. **a** Scatter plot of experimental and back-calculated ^1H, ^{15}N pseudocontact shifts (PCS) obtained from ^{15}N-labeled samples of IL1β-S2R2, IL1β-R2 and IL1β-S2 measured at 20 °C. **b** Axial and rhombic components of the Δχ-tensor and the respective metal position fitted from the ^1H, ^{15}N-PCS obtained for IL1β-S2R2, IL1β-R2 and IL1β-S2 against the Il1β-wild type structure. **c** The location of residues for which ^1H, ^{15}N-PCS could be obtained and analyzed for IL1β-S2R2 are shown as *orange spheres*. The determined positions of the two lanthanides are shown as *green spheres*

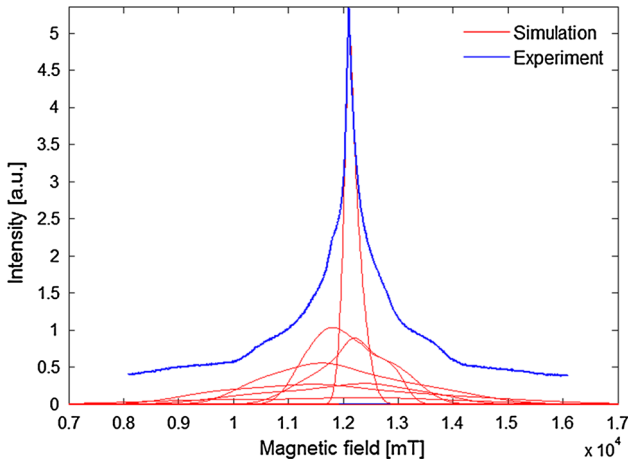

Fig. 6 Calculation of the Q-band EPR spectrum of Gd^{3+} at 10 K using EasySpin (Stoll and Schweiger 2006). Simulated transitions are separately shown (*in red*) as well as the experimental EPR spectrum of IL1β-S2R2 (*in blue*). Parameters used for the calculation are D = 1800 MHz, E = 400 MHz and a Gaussian distribution of 2/3 for both parameters. Experimental trace is rescaled for better visualization

procedure of adding additional data points for the single-loop-LBT mutants might not be necessary in cases where two-loop-LBTs are being used at different sites in multi-domain protein complexes. The position of the lanthanides will be further separated and line broadening due to the PRE might only affect signals close to the lanthanides, resulting in a higher number of detectable PCS. The advantage of using the two-loop-LBT approach is that one only needs to design and prepare a single protein construct and use it for both PELDOR and NMR spectroscopy.

We argue that the combination of single- and two-loop-LBT constructs might also be beneficial for the study of interdomain motions, as the combined dataset of PCSs yields an over determination of the experimental parameters, which allows for thorough probing of the relative motions of the individual $\Delta\chi$-tensor frames. Furthermore, the facile handling of the protein-LBT constructs and the remarkably precise distances obtainable by Gd^{3+}–Gd^{3+} PELDOR measurements make the encodable two-loop-LBT approach particularly suited for augmenting and cross validating studies on the structure and dynamics of multi-domain complexes.

Acknowledgments We thank Dmitry Akhmetzyanov for helpful discussions. This work was supported by Deutsche Forschungsgemeinschaft (DFG) in collaborative research centers 807 and 902. H.S. and T.P. are members of the DFG-funded cluster of excellence: macromolecular complexes and BMRZ is supported by the state of Hesse. K.N.A and B.I. acknowledge the support of NSF Grant MCB 0744415.

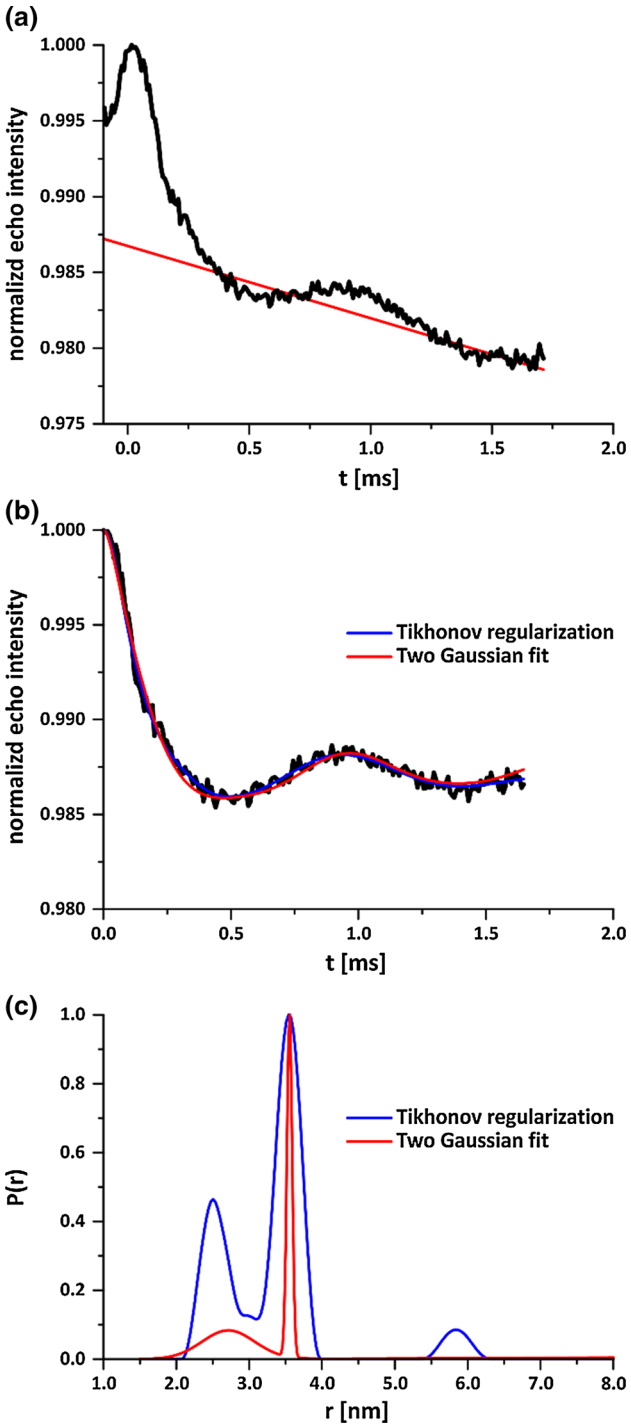

Fig. 7 Q-band PELDOR traces of 80 μM IL1β-S2R2 in 80 % buffer/20 % glycerol at 10 K. **a** Normalized PELDOR traces (*black*) and fitted background correction (*red*). Raw trace was cut at the end due to pulse overlap (Figure S8). **b** Background-corrected PELDOR traces (*black*) and interpolations obtained either from Tikhonov regularization (*blue*) or Two Gaussian fit (*red*). **c** Distance distributions using DeerAnalysis2013 (Jeschke et al. 2006) with the maximum at 3.55 nm and the Full Width at Half Height (FWHH) for the Tikhonov Regularization of about 0.5 nm

References

Alonso-García N, García-Rubio I, Manso JA et al (2015) Combination of X-ray crystallography, SAXS and DEER to obtain the structure of the FnIII-3,4 domains of integrin α6β4. Acta Crystallogr D Biol Crystallogr 71:969–985. doi:10.1107/S1399004715002485

Barthelmes K, Reynolds AM, Peisach E et al (2011) Engineering encodable lanthanide-binding tags into loop regions of proteins. J Am Chem Soc 133:808–819. doi:10.1021/ja104983t

Bentrop D, Bertini I, Cremonini MA et al (1997) Solution structure of the paramagnetic complex of the N-terminal domain of calmodulin with two Ce3 + ions by 1H NMR. Biochemistry 36:11605–11618. doi:10.1021/bi971022+

Bernstein FC, Koetzle TF, Williams GJ et al (1977) The Protein Data Bank. A computer-based archival file for macromolecular structures. Eur J Biochem 80:319–324. doi:10.1016/S0022-2836(77)80200-3

Bertini I, Janik MB, Lee YM et al (2001) Magnetic susceptibility tensor anisotropies for a lanthanide ion series in a fixed protein matrix. J Am Chem Soc 123:4181–4188

Bertini I, Luchinat C, Parigi G (2002) Magnetic susceptibility in paramagnetic NMR. Prog Nucl Magn Reson Spectrosc 40:249–273. doi:10.1016/S0079-6565(02)00002-X

Dalaloyan A, Qi M, Ruthstein S et al (2015) Gd(iii)–Gd(iii) EPR distance measurements—the range of accessible distances and the impact of zero field splitting. Phys Chem Chem Phys 17:18464–18476. doi:10.1039/C5CP02602D

Duss O, Michel E, Yulikov M et al (2014) Structural basis of the non-coding RNA RsmZ acting as a protein sponge. Nature 509:588–592. doi:10.1038/nature13271

Duss O, Yulikov M, Allain FH, Jeschke G (2015) Combining NMR and EPR to determine structures of large RNAs and protein–RNA complexes in solution. Methods Enzymol 558:279–331. doi:10.1016/bs.mie.2015.02.005

Garbuio L, Bordignon E, Brooks EK et al (2013) Orthogonal Spin Labeling and Gd(III)–nitroxide distance measurements on bacteriophage T4-lysozyme. J Phys Chem B 117:3145–3153. doi:10.1021/jp401806g

Göbl C, Madl T, Simon B, Sattler M (2014) NMR approaches for structural analysis of multidomain proteins and complexes in solution. Prog Nucl Magn Reson Spectrosc 80:26–63. doi:10.1016/j.pnmrs.2014.05.003

Goldfarb D (2014) Gd^{3+} spin labeling for distance measurements by pulse EPR spectroscopy. Phys Chem Chem Phys 16:9685. doi:10.1039/c3cp53822b

Gordon-Grossman M, Kaminker I, Gofman Y et al (2011) W-Band pulse EPR distance measurements in peptides using Gd^{3+}–dipicolinic acid derivatives as spin labels. Phys Chem Chem Phys 13:10771. doi:10.1039/c1cp00011j

Hass MA, Ubbink M (2014) Structure determination of protein–protein complexes with long-range anisotropic paramagnetic NMR restraints. Curr Opin Struct Biol 24:45–53. doi:10.1016/j.sbi.2013.11.010

Jeschke G, Chechik V, Ionita P et al (2006) DeerAnalysis2006—a comprehensive software package for analyzing pulsed ELDOR data. Appl Magn Reson 30:473–498. doi:10.1007/BF03166213

Keizers PHJ, Ubbink M (2011) Paramagnetic tagging for protein structure and dynamics analysis. Prog Nucl Magn Reson Spectrosc 58:88–96. doi:10.1016/j.pnmrs.2010.08.001

Lapinaite A, Simon B, Skjaerven L et al (2013) The structure of the box C/D enzyme reveals regulation of RNA methylation. Nature 502:519–523. doi:10.1038/nature12581

Loscha KV, Herlt AJ, Qi R et al (2012) Multiple-site labeling of proteins with unnatural amino acids. Angew Chem Int Ed 51:2243–2246. doi:10.1002/anie.201108275

Lueders P, Jeschke G, Yulikov M (2011) Double electron–electron resonance measured between Gd^{3+} ions and nitroxide radicals. J Phys Chem Lett 2:604–609. doi:10.1021/jz200073h

Lueders P, Jäger H, Hemminga MA et al (2013) Distance measurements on orthogonally spin-labeled membrane spanning WALP23 polypeptides. J Phys Chem B 117:2061–2068. doi:10.1021/jp311287t

Lynch M (2013) Evolutionary diversification of the multimeric states of proteins. Proc Natl Acad Sci U S A 110:E2821–E2828. doi:10.1073/pnas.1310980110

Mackereth CD, Madl T, Bonnal S et al (2011) Multi-domain conformational selection underlies pre-mRNA splicing regulation by U2AF. Nature 475:408–411. doi:10.1038/nature10171

Martin LJ, Hähnke MJ, Nitz M et al (2007) Double-lanthanide-binding tags: design, photophysical properties, and NMR applications. J Am Chem Soc 129:7106–7113. doi:10.1021/ja070480v

Matalon E, Huber T, Hagelueken G et al (2013) Gadolinium(III) spin labels for high-sensitivity distance measurements in transmembrane helices. Angew Chem Int Ed 52:11831–11834. doi:10.1002/anie.201305574

Pannier M, Veit S, Godt A et al (2000) Dead-time free measurement of dipole–dipole interactions between electron spins. J Magn Reson 142:331–340. doi:10.1006/jmre.1999.1944

Potapov A, Song Y, Meade TJ et al (2010) Distance measurements in model bis-Gd(III) complexes with flexible "bridge". Emulation of biological molecules having flexible structure with Gd(III) labels attached. J Magn Reson 205:38–49. doi:10.1016/j.jmr.2010.03.019

Raitsimring AM, Gunanathan C, Potapov A et al (2007) Gd^{3+} complexes as potential spin labels for high field pulsed EPR distance measurements. J Am Chem Soc 129:14138–14139. doi:10.1021/ja075544g

Russo L, Maestre-Martinez M, Wolff S et al (2013) Interdomain dynamics explored by paramagnetic NMR. J Am Chem Soc 135:17111–17120. doi:10.1021/ja408143f

Schiemann O, Prisner TF (2007) Long-range distance determinations in biomacromolecules by EPR spectroscopy. Q Rev Biophys 40:1. doi:10.1017/S003358350700460X

Schmitz C, Stanton-Cook MJ, Su X-C et al (2008) Numbat: an interactive software tool for fitting Deltachi-tensors to molecular coordinates using pseudocontact shifts. J Biomol NMR 41:179–189. doi:10.1007/s10858-008-9249-z

Silvaggi NR, Martin LJ, Schwalbe H et al (2007) Double-lanthanide-binding tags for macromolecular crystallographic structure determination. J Am Chem Soc 129:7114–7120. doi:10.1021/ja070481n

Song Y, Meade TJ, Astashkin AV et al (2011) Pulsed dipolar spectroscopy distance measurements in biomacromolecules labeled with Gd(III) markers. J Magn Reson 210:59–68. doi:10.1016/j.jmr.2011.02.010

Stoll S, Schweiger A (2006) EasySpin, a comprehensive software package for spectral simulation and analysis in EPR. J Magn Reson 178:42–55. doi:10.1016/j.jmr.2005.08.013

Studier FW (2005) Protein production by auto-induction in high density shaking cultures. Protein Expr Purif 41:207–234. doi:10.1016/j.pep.2005.01.016

Tamm LK, Lai AL, Li Y (2007) Combined NMR and EPR spectroscopy to determine structures of viral fusion domains in membranes. Biochim Biophys Acta Biomembr 1768:3052–3060. doi:10.1016/j.bbamem.2007.09.010

Wöhnert J, Franz KJ, Nitz M et al (2003) Protein alignment by a coexpressed lanthanide-binding tag for the measurement of residual dipolar couplings. J Am Chem Soc 125:13338–13339. doi:10.1021/ja036022d

Wolfram Research Inc., (2014) Mathematica version 10.0. Champaign

Yagi H, Banerjee D, Graham B et al (2011) Gadolinium tagging for high-precision measurements of 6 nm distances in protein assemblies by EPR. J Am Chem Soc 133:10418–10421. doi:10.1021/ja204415w

Yulikov M, Lueders P, Farooq Warsi M et al (2012) Distance measurements in Au nanoparticles functionalized with nitroxide radicals and Gd^{3+}–DTPA chelate complexes. Phys Chem Chem Phys 14:10732. doi:10.1039/c2cp40282c